16TH EUROPEAN CONFERENCE ON EARTHQUAKE ENGINEERING THESSALONIKI 18 - 21 JUNE 2018

VIBRATION CHARACTERISTIC OF A TYPICAL RESIDENTIAL BUILDING IN KATHMANDU: OPERATIONAL MODAL ANALYSIS AND FINITE ELEMENT MODELLING

Yoshio SAWAKI[1], Rajesh RUPAKHETY[2], Símon ÓLAFSSON[3]

ABSTRACT

System identification was conducted to estimate the fundamental vibration period and damping ratio of a residential building in Kathmandu. Ground motion and structural response due to aftershocks of the 2015 Gorkha Earthquake, as well as noise data triggered by ambient vibration were used to identify the dynamic properties of the structure. The identification is based on non-parametric spectral methods as well as parametric methods. Using aftershocks and triggered noise, the fundamental period of the building was found to be in the range of 0.23-0.3s. An empirical relation available in the literature predicts a fundamental period of 0.25s for the building being studied. It can be thus concluded that the fundamental period can be estimated with confidence. The damping ratio, however, showed greater variation. Statistical analysis by using auto-regressive with exogenous input (ARX) gave similar results as the non-parametric methods. The damping ratio estimated by ARX models was found to be closer to a generally expected value of 3-5%. In addition, a finite element model consisting of three dimensional beam-column elements and compression diagonal struts was created. The finite element model had a fundamental period of 0.26s, which is close to the value predicted by system identification.

Keywords: System Identification; 2015 Gorkha Earthquake; Ambient Vibration; Operational Modal Analysis; Finite Element Modelling

1. INTRODUCTION

Dynamic structural properties such as fundamental period and damping ratio are important information for designing earthquake-resistant structures, assessing structural damages after an earthquake, retrofitting structures efficiently and so on. Proper evaluation of these properties has ongoing interest in both engineering practice and scientific research. System identification is a method to evaluate such dynamic structural properties by using the measurements of structural response and excitation, if available. Mainly, there are two genres of the mathematical methods for system identification, non-parametric methods (Söderström et al., 1989) and parametric methods (Jenkins et al., 1969). Non-parametric method, for example spectral analysis, rely on visual inspection or curve fitting of spectral contents of recorded motion. On the other hand, parametric models, for example auto-regressive with exogenous input (ARX) model, rely on time-domain modelling of linear systems the parameters of which are calibrated using recorded excitation and response data (see, for example, Ljung, 1999). A more detailed review of structural system identification is provided by Alvin et al. (2003).
In this study, both non-parametric and parametric methods are used for system identification of a residential building in Kathmandu, Nepal. The building was shaken by the 2015 Gorkha Earthquake (see, for example, Rupakhety et al., 2017) and its aftershocks. Aftershocks recorded at the ground floor

[1]Research Student, Earthquake Engineering Research Centre, University of Iceland, Austurvegur 2a, 800 Selfoss, Iceland, yoshio@hi.is
[2]Research Professor, Earthquake Engineering Research Centre, University of Iceland, Austurvegur 2a, 800 Selfoss, Iceland, rajesh@hi.is
[3]Research Professor, Earthquake Engineering Research Centre, University of Iceland, Austurvegur 2a, 800 Selfoss, Iceland, simon@hi.is

and the roof of the building as well as noise data triggered by ambient vibration are used for system identification. Furthermore, a finite element model (FEM) of the building is created for comparing its modal properties with those obtained from system identification.

2. CASE-STUDY BUILDING

The residential building being studied is situated in Tyanglaphat, Kathmandu, Nepal. The building is made of reinforced concrete frames, cast in situ. The floors are also reinforced concrete and cast in situ. Both exterior and interior walls are brick masonry with cement/sand mortar. The building is 4-storey high with a floor height of 3.15m. The strength of concrete (f_{ck}) used in the frame and floor slab is 20 MPa, and the tensile strength of steel reinforcement is 415 MPa (NBC 201, 1994). Ground floor and roof plan of the building are shown in Figure 1, with indications of the locations of accelerometers used to record vibration data. The unit on the roof was installed in the main structural system of the building at the concrete floor of the fourth level. The blue arrows in Fig 1 indicate the horizontal directions of the sensors (channel 1 and 2).

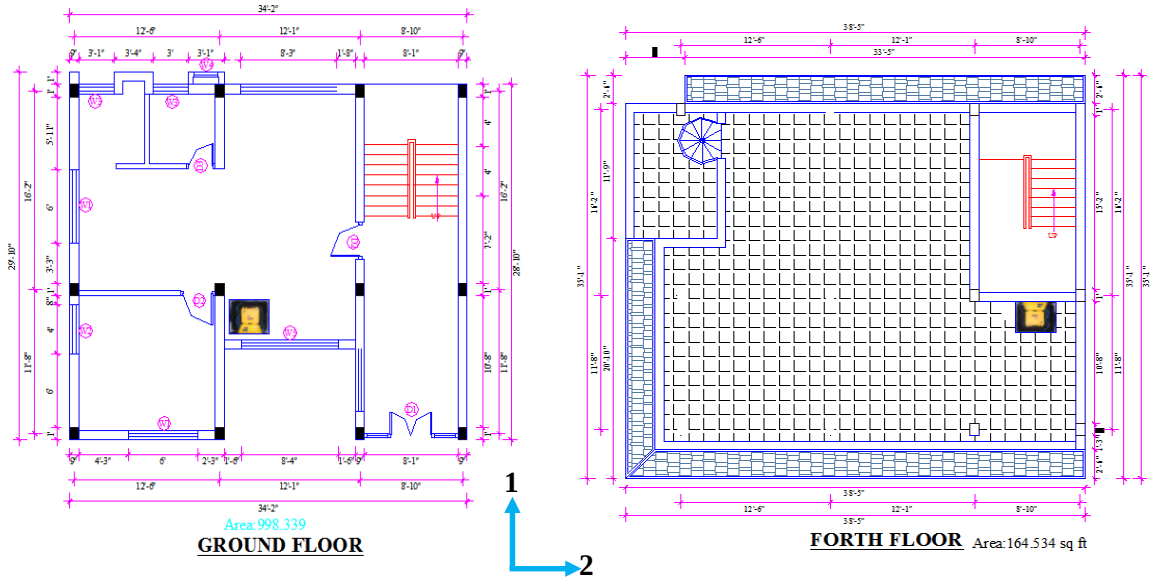

Figure 1. Ground floor and roof plan of the building being studied. The small yellow pictures indicate the locations of accelerometers installed in the building

3. DATA

3.1 Aftershock data

The three aftershocks used in this study are listed in Table 1. Three component acceleration time series were recorded during each of these aftershocks. The horizontal components are called as channel-1 and channel-2 (see Fig 1 for their orientations) and the vertical one is called as channel-3 hereafter. Only these three aftershocks were recorded simultaneously by the unit on the ground floor and roof, although many aftershocks had occurred since the accelerometers were installed. On the other hand, many more aftershocks were registered by the unit on the ground floor. This is, in part, due to malfunctioning of the triggering system of the unit on the roof.

3.2 Ambient vibration data

Noise data triggered by ambient vibration between 6 October 2015 to 21 June 2016 are considered in this study. The total number of triggered events is 825. As many of them had peculiar drift or were of

very short duration, they were not used for further analysis. It was also noticed that noise data recorded by channel-1 was of lower quality, for example, had severe drift, spiky peaks, etc. Such deficiencies were not present in channel-2 records. In total, 362 triggered events recorded by channel-2 of the roof unit is used in spectral analysis.

Table 1. List of aftershocks of 2015 Gorkha Earthquake

No.	Date	Time (UTC)	PGA (%g)	Magnitude M_w	Latitude (°, NSC)	Longitude (°, NSC)	Depth (km)
1	21/06/2016	5:48	0.6	3.6	27.93	85.21	10
2	28/05/2016	3.43	1.1	4.7	27.94	85.50	10
3	31/10/2015	9:37	0.1	-	28.03	85.23	-

4. NON-PARAMETRIC ANALYSIS

4.1 Spectral analysis using aftershocks

Horizontal acceleration time series at ground and roof were windowed to cover 90% of cumulative Arias Intensity. The selection of the widow was also verified visually, assuming that a stationary signal implies a linear build-up of Arias Intensity with time. The windowed time series were tapered with a Tukey window accommodating the taper over 15% of the total length of the signals. The signals were then band-pass filtered using a 4th-order zero-phase Butterworth filter in the frequency band of 1-15 Hz. The power spectral density (PSD) of the filtered signal was estimated with Welch's algorithm dividing the signal into 5 segments with 50% overlap. The squared amplitude $|H(f)|^2$ of frequency response function of the building is then estimated as

$$|H(f)|^2 = S_{yy}(f)/S_{xx}(f) \quad (1)$$

where $S_{yy}(f)$ and $S_{xx}(f)$ are the Welch's PSD estimated of the roof and ground acceleration, respectively. An example of normalized $|H(f)|^2$, estimated using this method, is shown in Figure 2. The fundamental frequency ($f_n = 1/T_0$, T_0: fundamental period) is selected as the frequency of the first peak (read circle in Fig 2). The two frequencies f_1 and f_2 ($f_2 > f_1$) (black circles in Fig 2) corresponding to the half-power bandwidth are used to estimate the damping ratio (ξ) . The relation between bandwidth and damping ratio is given by the following equation (Papagiannopoulos et al., 2011).

$$\xi = (f_2 - f_1)/2f_n \quad (2)$$

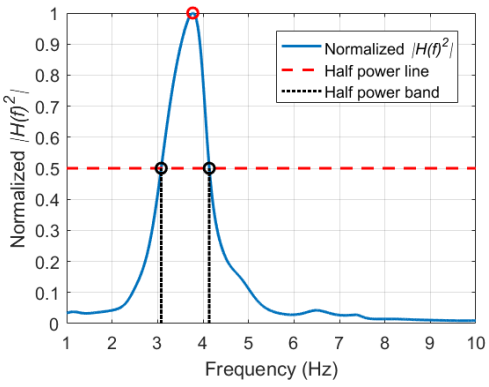

Figure 2. Example of a normalized $|H(f)|^2$ computed from the channel-2 data of aftershock no.1

4.2 Spectral analysis using triggered noise

Assuming that the excitation is a white noise with a constant PSD (P_0) at all frequencies of interest, the squared amplitude $|H(f)|^2$ of frequency response function of the building is equal to the PSD of the roof motion (excitation) scaled by P_0.

$$|H(f)|^2 = S_{yy}(f)/P_0 \tag{3}$$

Although P_0 is unknown, the fundamental frequency and damping ratio of the building can be estimated because P_0 is merely a scaling factor. For this analysis, 362 triggered events were used. The triggered noise data were windowed to cover 5% and 95% of cumulative Arias Intensity, and PSD was estimated in the same way as that described in the previous section. As a different approach, periodogram PSD estimated was carried out for each noise data, and ensemble averaged PSD was used to estimate the normalized $|H(f)|^2$.

The horizontal to vertical spectral ratio (HVSR) provides an estimate of the squared amplitude of frequency response function of a structure, assuming that the building is very stiff in the vertical direction compared to the horizontal direction. This method is frequently used for estimating the resonance site frequencies (see, for example, Nakamura, 2008). It has also been found to be effective to estimate fundamental frequency of a building using ambient vibration measurement (see, for example, Gallipoli et al., 2009; Gallipoli et al., 2010). In HVSR method, it is common to record a few tens of minutes of ambient vibrations continuously. For this application, however, triggered noise data with different duration were used. Welch's algorithm, as mentioned in the previous section, is effective for smoothing PSD before computing the HVSR. As an alternative method, ensemble averaging is useful to reduce the variability of PSD estimate. Under the assumption that the individual event is a realization of the same random process, periodogram PSDs of noise data can be averaged to obtain a smoother mean PSD. In this study, 282 triggered noise data were used to estimate PSD in two different ways. In the first method, HVSR spectrum from each noise data was estimated by using Welch's PSD of the horizontal (channel-2) and vertical (channel-3) signals. In the second method, the mean horizontal PSD ($\overline{S_{yy}}(f)$) and vertical PSD ($\overline{S_{zz}}(f)$) were obtained using periodogram estimates. The average HVSR spectrum, which can be considered to be proportional to $|H(f)|^2$, is obtained as

$$|H(f)|^2 \propto HVSR = \overline{S_{yy}}(f)/\overline{S_{zz}}(f) \tag{4}$$

5. PARAMETRIC ANALYSIS

5.1 ARX model

Parametric ARX models were calibrated by using the ground and roof motions. The ARX model uses the input signal effect $u(t)$ and the output signal $y(t)$ to calibrate a system. The ARX(n_a, n_b) model is expressed by the following equation.

1.

$$y(t) = -a_1 y(t-1) - \cdots - a_{n_a} y(t-n_a) + b_1 u(t-n_k) + \cdots + b_{n_b} u(t-n_k-n_b+1) + e(t) \tag{5}$$

where a_{n_a} and b_{n_b} are the model paremeters; n_a and n_b are the model orders of polynomial; and $e(t)$ represents a white-noise. An equivalent representation of the discrete-time ARX model is

$$A(z)y(t) = B(z)u(t) + e(t) \tag{6}$$

where

$$A(z) = 1 + a_1 z^{-1} + \cdots + a_{n_a} z^{-n_a} \tag{7}$$

$$B(z) = b_1 + b_2 z^{-1} + \cdots + b_{n_b} z^{-n_b+1} \tag{8}$$

The transfer function $G(z)$ of the ARX model, obtained by taking the z-transform, is a rational function of z and given by

$$G(z) = B(z)/A(z) \tag{9}$$

The fundamental angular frequency ω_n and damping ratio ξ are obtained from the ith poles (λ_i) of the transfer function $G(z)$ by using the equations

$$\omega_n = |\ln\lambda_i / T_s| \tag{10}$$

$$\xi = -\cos(\arg(\ln\lambda_i)) \tag{11}$$

where T_s is the sampling interval.

5.2 Optimal model order

The model order of the ARX model was determined so that the model is as simple as possible and the transfer function has all its poles within the unit circle. Akaike's information criterion (AIC) (Akaike, 1974) was applied for selecting the optimal model order. An example using the channel 2 signal of aftershock no. 1 is shown in Figure 3(a). It can be seen that AIC value decreases with increasing model order and saturates for a model of order 50. However, the decrease of AIC is rather slow after some model order. Therefore, an ARX(n_a,n_b) whose AIC value goes below 90% line was temporarily selected as the optimal model order. In Fig 3(a), for example, 19th model order was expected to be optimal. The transfer function of ARX(19,19) was then checked to confirm that all of its poles are within the unit circle. The normalized root mean square error (NRMSE) of the model was then verified to be positive. In Figure 3(b) and 3(c), all of the poles are within the unit circle and NRMSE is positive.

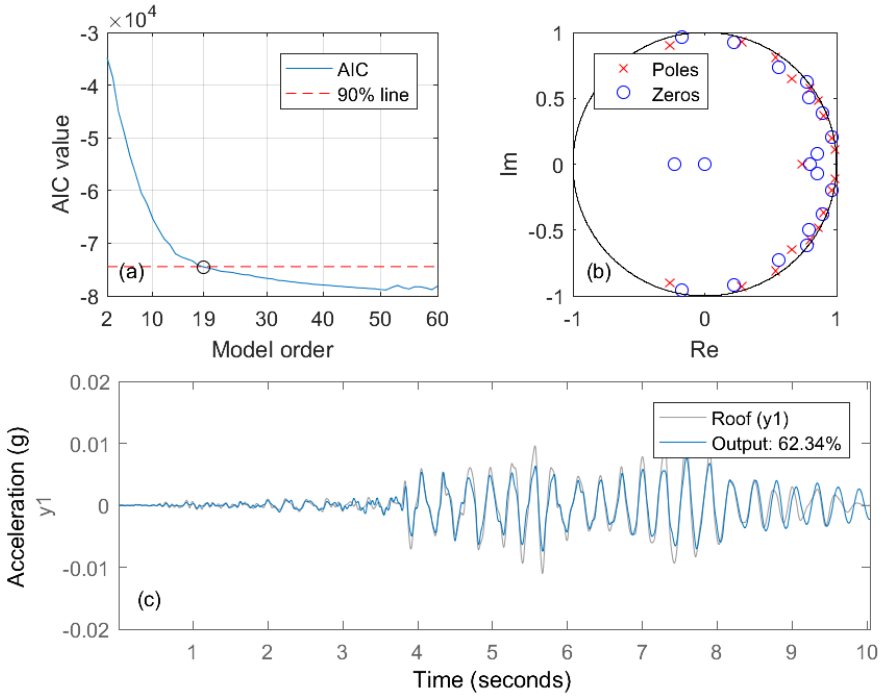

Figure 3. Selection of the optimal model order using channel-2 of aftershock no. 1: (a) AIC values for various model orders with 90% line of the minimum value, and the black circle represents 19th model order; (b) Pole-zero plot of ARX(19,19) model; (c) Output of ARX(19,19) model (blue) and the aftershock recorded at the roof (grey). The NRMSE is 62.34% in this case

6. FINITE ELEMENT ANALYSIS

A finite element model (FEM) of the building was created using SAP2000 (CSI, 2016) to investigate its general vibration characteristics. The FEM consists of three dimensional beam-column elements to model the RC frame and diagonal compression struts to model the brick masonry wall. The modulus of elasticity of RC column and beam E_c (ATC-40, 1996 and FEMA-273, 1997) and compressive strut $E_{m\theta}$ (Crisafulli, 1997) are estimated as,

$$E_c = 5000\sqrt{f_{ck}} \tag{12}$$

$$E_{m\theta} = 1000 f_{m\theta} \tag{13}$$

where f_{ck} is the characteristic compressive strength of concrete at 28 days, taken here as 20MPa (NBC 201, 1994) and $f_{m\theta}$ is the mean diagonal compressive strength, taken here as 15kPa (Bal et at., 2006). Other structural properties are listed in Table 2. To model the diagonal compressive struts, their strut width w was determined using the following equation (Holmes, 1961).

$$w = d/3 \tag{14}$$

where d is a diagonal length of the infill wall.
If an infill wall has an opening, the strut width is reduced by the strut width reduction factor ρ_w (Mondal et al., 2008), given by

$$\rho_w = 1 - 2.6\alpha_{c0} \tag{15}$$

where α_{c0} is the fraction of opening area and wall area. The FEM is shown in Figure 4.

Table 2. Properties of structural components

Structural Part	Material	Density ($\mathbf{kN/m^3}$)	Modulus of Elasticity (MPa)	Poisson's Ratio
Beam	RC	24.5	22.361	0.20
Column	RC	24.5	22.361	0.20
Strut	Brick masonry	18.85	1.5	0.19

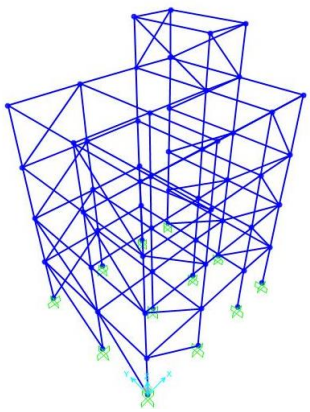

Figure 4. Finite element model of the building

7. RESULTS AND DISCUSSION

7.1 Results from non-parametric analysis using aftershocks

In Figure 5, the normalized $|H(f)|^2$ of the building computed from PSD of channel-1 and -2 of three aftershocks are presented. The damping ratio and fundamental period estimated from the normalized $|H(f)|^2$ are listed in Table 3. The results show that the fundamental period in channel-1 are in the range of 0.23s to 0.24s, and that in channel-2 are in the range 0.26s to 0.28s. Kocak et al. (2013) performed the finite element analysis of buildings with different configurations of infill walls and openings, and found that the fundamental period of such buildings was best predicted by the empirical equation given in Guler et al. (2009):

$$T_0 = 0.026H^{0.9} \tag{16}$$

where H is the height of the building in meters. According to this equation, the fundamental period of the building being studies is 0.25s, which is close to the period estimated from spectral analysis presented here. The estimated damping ratio varied in the range of 4% to 14%. It is important to mention that the level of smoothing carried out to estimate the PSD directly affects the damping ratio. If the smoothing is excessive the peak becomes wider, which leads to larger damping ratio.

Table 3. Damping ratio and fundamental period estimates from channel-1 and -2 of the three aftershocks

Data No.	Damping Ratio of Ch-1 (%)	Fundamental Period of Ch-1 (s)	Damping Ratio of Ch-2 (%)	Fundamental Period of Ch-2 (s)
1	11.7108	0.2396	13.9829	0.2649
2	4.2974	0.2290	6.3081	0.2781
3	6.9367	0.2393	9.9296	0.2770

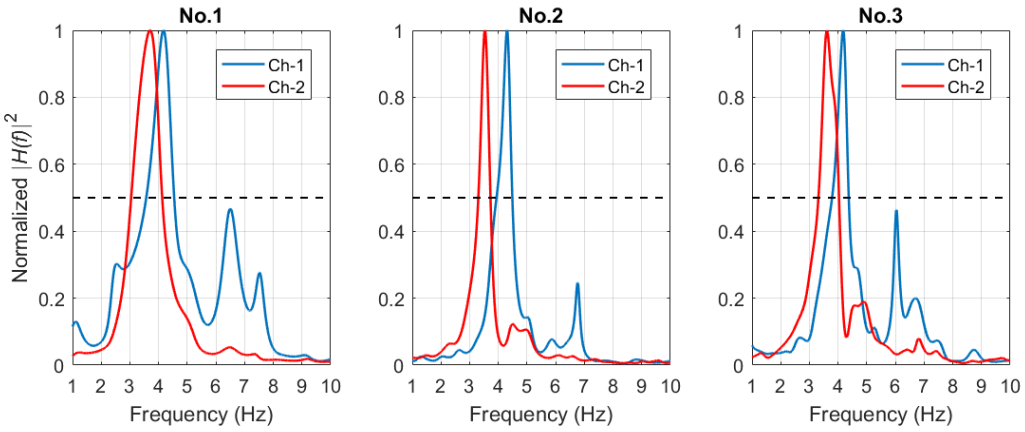

Figure 5. Normalized $|H(f)|^2$ of frequency response function of the building computed from PSD of channel-1 and -2 of each aftershock. The black-dashed line represents the half-power line

7.2 Results from non-parametric analysis using triggered noise data

Figure 6 shows 362 normalized $|H(f)|^2$ computed from channel-2 data of roof vibration. Figure 7 shows the normalized $|H(f)|^2$ obtained from HVSR using 282 events recorded by the roof sensor. The estimated damping ratios and fundamental periods are listed in Table 4. Fig 6(a) shows the histograms of the damping ratio and fundamental period based on Welch's PSD estimate. The mean damping ratio

and fundamental period are 4.7% and 0.3s, respectively. Ensemble averaged PSD resulted in $|H(f)|^2$ shown in Fig 6(b). The damping ratio and fundamental period estimated from these spectra are 4.5% and 0.3s, respectively. Fig 7(a) shows the histograms of damping ratio and fundamental period obtained from HVSR method using Welch estimates of PSD. The mean damping ratio and fundamental period are 8% and 0.3s. Ensemble averaged PSD of horizontal and vertical motion is presented in Fig 7(b). The resulting HVSR is shown in Fig 7(c). The damping ratio and fundamental period estimated from HVSR are 8.5% and 0.3s, respectively.

Compared to the damping ratio estimated from the HVSR, the one estimated from horizontal PSD was found to lie in the expected range of 3% and 5%. The damping ratio estimated from aftershocks and triggered noise data were largely variable. This result is in part related to the uncertainties due to the level of smoothing PSD, which has a direct impact on half-power band width. Fundamental periods estimated from different non-parametric methods using triggered noise data all were found to be around 0.3s. This is slightly larger than the results from aftershocks and 0.25s given by Eq. (16). The results indicate that ambient vibration measurement provides an estimate of a building fundamental period similar to that obtained from earthquake aftershocks with much higher amplitude.

Table 4. Mean values and standard deviations σ of the damping ratio and fundamental period

Channels	PSD Estimate	No. of Time Series	Mean Damping Ratio (%)	σ of Damping Ratio	Mean Fundamental Period (s)	σ of Fundamental Period
2	Welch's	362	4.7	2.0270	0.3	0.008
2	Ensemble Average	362	4.5	-	0.3	-
2&3	Welch's	282	8.0	3.4792	0.3	0.012
2&3	Ensemble Average	282	8.5	-	0.3	-

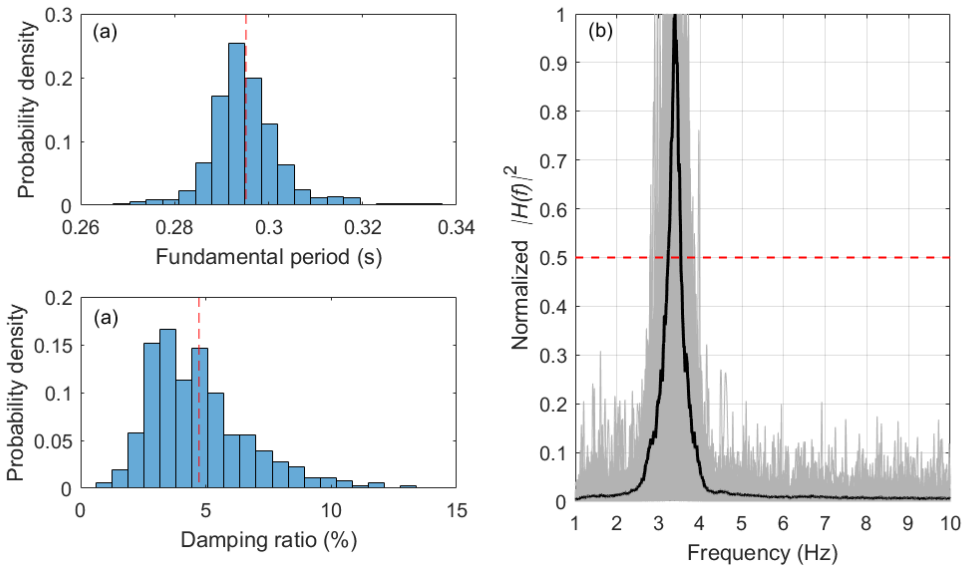

Figure 6. Results from 362 normalized $|H(f)|^2$: (a) Histograms of the fundamental period and damping ratio. The red-dashed line on each figure is the mean value; (b) Normalized $|H(f)|^2$ of 362 triggered noise based on periodogram PSD estimate. The solid black line represents the normalized ensemble average

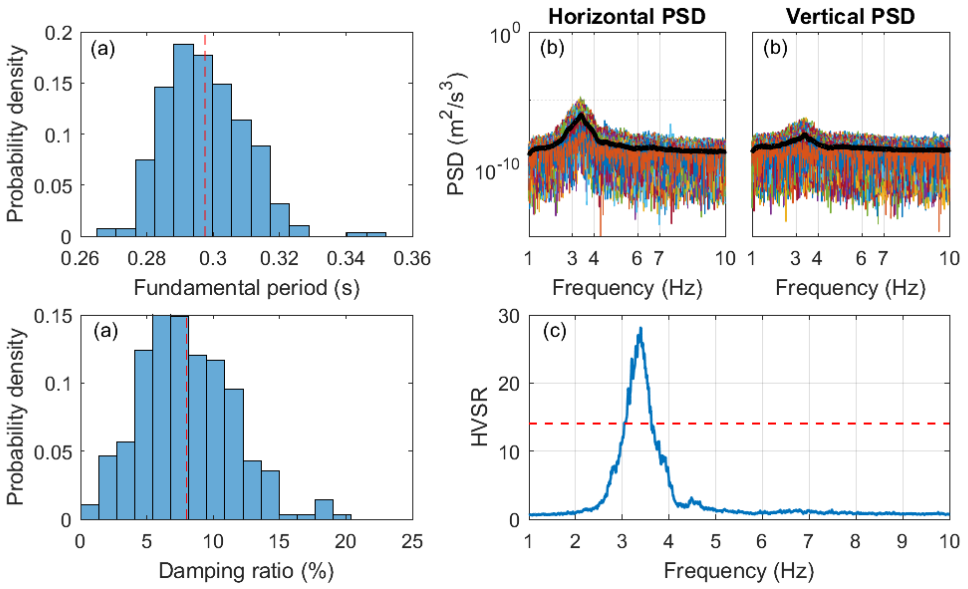

Figure 7. Results from 282 HVSR: (a) Histograms of the fundamental period and damping ratio. The red-dashed line on each figure is the mean value; (b) Ensemble average horizontal and vertical PSD (black solid line on each figure); (c) HVSR obtained from ensemble average PSD. The red-dashed line represents half the value of the maximum HVSR

7.2 Results from parametric analysis

The optimal ARX models were calibrated using ground and roof acceleration time series of the three aftershocks. In this analysis, the two horizontal components were treated separately. The damping ratio and fundamental period estimated from the ARX models are shown in Table 5. The ARX model of channel-1 of No. 1 aftershock is not reliable because its AIC value was too large. The ARX model of channel-1 of No. 3 aftershock is of too high order. Therefore, these two models are considered unrealistic.

The damping ratio computed from the ARX models is in the range of 2.6% and 4.7 % and has much less variance compared to the results from aftershocks listed in Table 3. All of these values are close to or within 3% to 5%, a generally expected damping ratio of the building. The fundamental period varies from 0.24s to 0.30s and is same as the results in Table 3. It was found that the damping ratio computed from ARX models resulted in lower uncertainty than the one estimated in the parametric analysis.

Table 5. Damping ratio and fundamental period obtained from each optimal ARX model

Data No.	Channel	Optimal Order of ARX model	Damping Ratio (%)	Fundamental Period (s)
1	1	(4,4)	1.99	0.2271
	2	(19,19)	4.68	0.2775
2	1	(19,19)	3.92	0.2420
	2	(19,19)	2.64	0.2962
3	1	(59,59)	9.27	0.3382
	2	(19,19)	2.74	0.2795

7.3 Results from finite element analysis

Modal analysis of the FEM model resulted in a fundamental period of 0.26s and a second mode period of 0.16s. This is in agreement with Equation (16) and the results from system identification. It is interesting to note that the 2nd-mode frequency obtained from the modal analysis lies in the range between 6Hz and 7Hz, which was also seen in the normalized $|H(f)|^2$ of channel-1 of aftershocks shown in Fig 3. Figure 8 shows a comparison of the simulated (using FEM) and recorded response for aftershock no. 1. The simulated response in direction of channel-2 shows similar characteristics to the recorded motion. It has a predominant frequency between 3Hz and 4 Hz, like the recorded motion (see Fig. 5). On the other hand, although the Fourier amplitude of channel-1 data has its predominant frequency in the range of 3Hz and 4Hz, the predominant frequency of the simulated response lies between 6Hz and 7 Hz. This shows that the FEM is stiffer than the actual structure in the direction of channel-1. Results for other aftershocks showed similar characteristics. This indicates that modelling of masonry walls needs to be refined.

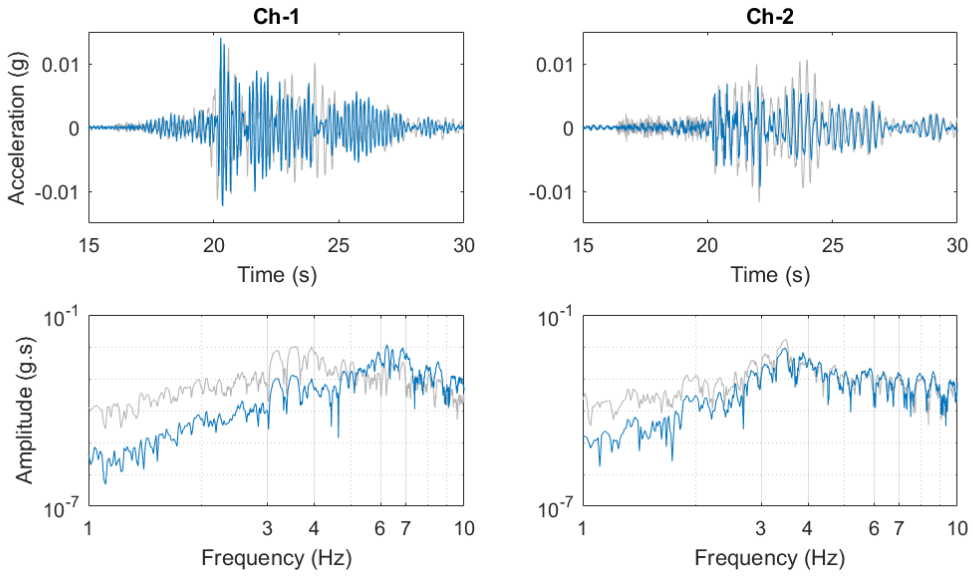

Figure 8. Acceleration and Fourier amplitude spectra at the roof in channel-1 and -2 direction for aftershock No. 1. The simulated response and recorded motion are plotted in blue and grey respectively.

8. CONCLUSIONS

The vibration characteristics of a typical residential building in Kathmandu, made of RC frame with brick masonry infill wall, were investigated through operational modal analysis (non-parametric and parametric) and finite element analysis. Using three aftershocks of the 2015 Gorkha Earthquake, the damping ratio and fundamental period of the building were estimated from the normalized $|H(f)|^2$ as well as the ARX model. The damping ratio estimated by the half-power bandwidth method using the normalized $|H(f)|^2$ had a large variance and lied in the range of 4% and 14%. Those computed from ARX models lied between 2.6% and 4.7%. Fundamental period of the building inferred from parametric and non-parametric methods were found to be similar. Using noise data triggered by ambient vibration, damping ratio and fundamental periods were estimated by using the normalized $|H(f)|^2$ and HVSR. In both cases, two approaches of spectral estimate were used; Welch's PSD estimate and ensemble averaging of periodogram PSD. The damping ratios obtained from the normalized $|H(f)|^2$ computed by both PSD estimates lied between 4.5% and 4.7%. However, the damping ratio estimated from HVSR were found to be much larger than expected—around 8%. Note that although the mean damping ratio was similar to what is generally expected there was considerable variation. Based on the results from non-parametric and parametric analysis, it can be concluded that ambient vibration measurement

provides an estimate of a building fundamental period similar to that obtained from earthquake aftershocks. Ambient vibration measurements can be used in either the framework of HVSR method or just the horizontal component of motion for estimating fundamental period of buildings. It would be desirable to use parametric model, such as ARX, to estimate more accurate damping ratio.
It was found that the result of the finite element model of the building in a fundamental period was close to those estimated from system identification. Although the finite element model was found sufficient to reproduce the overall characteristics of recorded aftershock motion, it had some deficiencies. The FEM simulated motion in one of the directions of the building had different frequency content than recorded motion. Although this did not result in large difference in peak motion, the FEM was stiffer than the actual building in this direction. This deficiency is most likely due to the inadequate modelling of the masonry walls. Since the percentage area of openings in the two directions of the building are very different, and because the FEM performed well in one of the directions, it can be inferred that the equation used for reduction of strut width is not accurate enough.

9. ACKNOWLEDGMENTS

The authors acknowledge financial support from University of Iceland Research Fund and the national power company of Iceland, Landsvirkjun. The first author acknowledges Ministry of Education, Culture, Sports, Science and Technology of Government of Japan for providing him the scholarship to support his research internship at the EERC. The authors thank Mr. Damodar Rupakhety for allowing us to install the accelerometers in his house and to use the collected data for the research presented here. Mr. Rajan Dhakal prepared the plans of the building presented here, and Dr. Benedikt Halldorsson helped in configuring the accelerometers; their contributions are gratefully acknowledged.

10. REFERENCES

Akaike H (1974). A new look at the statistical model identification, *IEEE Transactions Automatic Control*, AC-19:716-723.

Alvin KF, Robertson AN, Reich GW, Park KC (2003). Structural system identification: from reality to models, *Computers & structures*, 81(12):1149-76.

Applied Technology Council (ATC) (1996). *Seismic Evaluation and Retrofit of Concrete Buildings*, volumes 1 and 2, Report No. ATC-40, Redwood City, CA.

Bal, I., Crowley, H., Pinho, R. and Gulay, G. (2006). Structural Characterisation of Turkish R/C Building Stock for Loss Assessment Applications, *Proceedings of 1st European Conference of Earthquake Engineering and Seismology*, Geneva, paper n° 603.

Crisafulli, F.J. (1997). Seismic Behaviour of Reinforced Concrete Structures with Masonry Infills, *PhD Thesis*, University of Canterbury, New Zealand.

CSI (2016), SAP2000 Integrated Software for Structural Analysis and Design, Computers and Structures INC., Berkeley, California.

Federal Emergency Management Agency (FEMA) (1997). NEHRP Guidelines for the Seismic Rehabilitation of Buildings, *FEMA-273, 1997*, Washington, DC.

Gallipoli MR, Mucciarelli M, Vona M (2009). Empirical estimate of fundamental frequencies and damping for Italian buildings, *Earthquake Engineering and Structural Dynamics*, 38: 973-988.

Gallipoli MR, Mucciarelli M, Šket-Motnikar B, Zupanćić P, Gosar A, Prevolnik S, Herak M, Stipčević J, Herak D, Milutinović Z, Olumćeva T (2010). Empirical estimates of dynamic parameters on a large set of European buildings, *Bulletin of Earthquake Engineering*, 8: 593 – 607.

Goutam, Mondal and Sudhir, K. Jain (2008). Lateral Stiffness of Masonry Infilled Reinforced Concrete (RC) Frames with Central Openings, *Earthquake Spectra*, **24**, No. 3, 701-723.

Guler K, Yuksel E, Kocak A (2009). Estimation of the fundamental vibration period of existing RC buildings in Turkey utilizing ambient vibration records, *Journal of Earthquake Engineering*, 12(S2):140-150.

Holmes, M. (1961). Steel Frames with brickwork and concrete infilling, *Proceedings of the Institution of Civil Engineers*, **19**, 473-478 (eISSN 1753-7789).

Jenkins G M, Watt D G (1968). Spectral analysis and its application, Holden-Day, San Francisco.

Kocak A, Kalyoncuoglu A, Zengin B (2013). Effect of infill wall and wall openings on the fundamental period of RC buildings, *Earthquake Resistant Engineering Structures IX*, *WIT Transactions on The Built Environment*, 132:121-131, doi: 10.2495/ERES130101.

Ljung L (1999). System identification. John Wiley & Sons, Inc.

Ministry of Physical Planning and Works (1994). Nepal National Building Code (NBC 201): Mandatory Rules of Thumb Reinforced Concrete Buildings with Masonry Infill.

Nakamura Y (2008). On the H/V spectrum, *Proceedings of the 14th World Conference on Earthquake Engineering*, 12-17 October, Beijing, China.

National Seismological Centre (NSC) (2015). http://www.seismonepal.gov.np/ (last accessed 21 June 2015)

Papagiannopoulos G A, Hatzigeorgious G D (2011). On the use of the half-power bandwidth method to estimate damping in building structures, *Soil Dynamics and Earthquake Engineering*, 31:1075—1079.

Rupakhety R, Olafsson S, Halldorsson B (2017). The 2015 Mw 7.8 Gorkha Earthquake in Nepal and its aftershocks: analysis of strong ground motion, *Bulletin of Earthquake Engineering*, DOI: 10.1007/s10518- 017-0084-z.

Söderström T, Stoica P (1989). System identification, Prentice Hall International, Cambridge.

United States Geological Survey (USGD) (2015). http://earthquake.usgs.gov/earthquakes/eventpage/us20002926#general_summary (last accessed 21 June 2015)